processes

MDPI

*Article*

# Effect of Counterbody on Friction and Wear Properties of Copper-MgP-Graphite Composites Prepared by Powder Metallurgy

**Ruoxuan Li [1,*], Seiji Yamashita [1,*], Katsumi Yoshida [2] and Hideki Kita [1]**

[1] Department of Materials Process Engineering, Graduate School of Engineering, Nagoya University, Furo-cho, Chikusa-ku, Nagoya 464-8603, Japan; kita.hideki@material.nagoya-u.ac.jp
[2] Laboratory for Zero-Carbon Energy, Institute of Innovative Research, Tokyo Institute of Technology, 2-12-1, Ookayama, Meguro-ku, Tokyo 152-8550, Japan; k-yoshida@zc.iir.titech.ac.jp
* Correspondence: li.ruoxuan.a4@s.mail.nagoya-u.ac.jp (R.L.); yamashita.seiji@material.nagoya-u.ac.jp (S.Y.)

**Abstract:** The purpose of this study was to investigate the influence of different counterbodies against Cu/magnesium phosphate treated graphite (Cu-MgPG) composite materials to find the best material combination in terms of friction coefficient and specific wear amount. A Cu matrix composite reinforced with 10 vol% magnesium phosphate treated graphite and pure Cu powder were prepared by powder metallurgy techniques under the same consolidation processing condition. The friction and wear properties of the composites were investigated at 10 N using a pin-on-disc tribometer on $Al_2O_3$, SiC and SUJ2 bearing steel counterbodies. The Cu-MgPG/$Al_2O_3$ pair showed the lowest friction coefficient, but the specific wear rate tended to increase slightly when compared with Cu/$Al_2O_3$ pair. On the other hands, the Cu-MgPG/SUJ2 pair showed about the same specific wear rate as the Cu/SUJ2 pair, but the friction coefficient was significantly reduced. These phenomena are thought to be due to the fact that the added graphite acts as a solid lubricant during sliding and also suppresses the oxidation behavior of the sliding material.

**Keywords:** graphite; Magnesium Phosphate; sliding wear; copper-matrix composite; friction; wear; counterbody



**Citation:** Li, R.; Yamashita, S.; Yoshida, K.; Kita, H. Effect of Counterbody on Friction and Wear Properties of Copper-MgP-Graphite Composites Prepared by Powder Metallurgy. *Processes* **2022**, *10*, 804. https://doi.org/10.3390/pr10050804

Academic Editor: Sung-Churl Choi

Received: 24 March 2022
Accepted: 18 April 2022
Published: 19 April 2022



## 1. Introduction

Graphite as a common solid lubricant that is often added to metal materials to make new materials with self-lubricating properties [1–6].

Copper-graphite composites possess both copper and graphite properties, including excellent thermal and electrical conductivity, solid lubrication, low coefficient of thermal expansion and so on, which makes these composite widely used as a brush and bearing material in many applications [3,7]. In fact, components in this type of application are often exposed to high friction, temperature rise and environmental erosion [8]. The good friction properties of copper-graphite composites are often due to the fact that the graphite particles exposed on the surface of the composites act as lubricants during the friction process [9–11]. Considering that graphite is prone to oxidation in high temperature environments, the operating temperature range of ordinary copper-graphite composites is also limited.

In a previous work [12], it proposed a method to improve the oxidation resistance of graphite while maintaining the lubricating properties of graphite. In this study, the magnesium phosphate-treated graphite (MgPG) was used as a solid lubricating phase to mix with copper powder, and used powder metallurgy technique to make copper/magnesium phosphate-treated graphite composite materials (Cu-MgPG).

In the preparation of copper-graphite composite materials, many studies [9,13–16] have investigated the effect of the content of graphite added on the properties of the final composites. While this work aims to study the friction properties of composites made

of 10 vol% magnesium phosphate treated graphite and copper. Research [14] has shown that when the volume content of graphite is less than 50%, sintering temperature lies in 700 °C–950 °C to improve the metallurgy bonding between copper and copper in the material. At the same time, the raw material with treated graphite [12] used in this study was produced by sintered natural graphite with magnesium phosphate at 800 °C. Based on the above data, the sintering temperature of the composite material selected in this study was 800 °C.

Many scholars have studied the tribological properties of copper-graphite composite materials under different conditions, and the results show that the tribological behavior of copper-graphite composite materials is complex and dependent on external factors. These important external factors include applied load, sliding velocity, ambient temperature, humidity, and counterbody material. However, there are few studies on the effect of counterbody materials on the friction properties of copper-graphite composite materials.

In this study, powder metallurgy technique was used to prepare Cu-MgPG composite materials and a comparative sample of pure copper (Cu) materials prepared under the same conditions. Then we compared the physical properties, friction properties and surface microstructure of the pure copper materials and Cu-MgPG composites. In addition, in order to find the optimum tribopair combination of Cu and Cu-MgPG with the counterbody materials, the influence of the counterbody materials in terms of coefficient of friction and wear was investigated.

## 2. Materials and Methods

### *2.1. Preparation of the Samples*

The magnesium phosphate-treated graphite (MgPG) raw material used in this study was prepared according to the method of previous study [12]. The arithmetic average particle size of the magnesium phosphate-treated graphite (natural graphite powder, D50 = 93.16 μm; $Mg(H_2PO_4)_2 \cdot 4H_2O$, MW:290.34, JUNSEIKAGAKU) used in this work was 131.70 μm.

The composites were fabricated by powder metallurgy technique. 10 vol% MgPG powder and copper powder (Nilaco, Ginza, Tokyo, Japan) were dry-mixed with a bench kneader machine (Irie Shokai Co., Ltd., Tokyo, Japan) for 3 h. After mixing, the powder mixture was first cold pressed at 30 MPa in 35 mm × 35 mm square mold, and then hot-pressing in nitrogen flow (2 L/min) at 800 °C for 3 h with a uniaxial pressure of 40 kN. For comparison, parallel compacts made from pure copper powders were consolidated under the same conditions applied for the preparation of Cu-MgPG composites. All specimens were polished to get a mirror-effect and cleaned with acetone before every experiment. The polished surfaces were then observed by SEM (JEOL Ltd., JSM-7500F, Tokyo Japan). The typical SEM micrograph of the polished surface of Cu-MgPG composites and copper are shown in Figure 1. The magnesium phosphate-treated graphite particles dispersed in the copper matrix can be observed in Figure 1A.

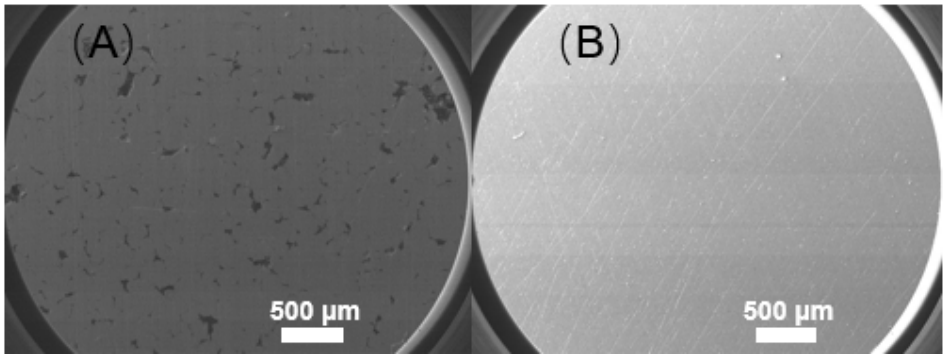


**Figure 1.** A typical SEM micrograph of the polished surface of (**A**) copper/MgP-graphite composites and (**B**) copper.

### 2.2. Physical Properties

The densities of the sintered copper/MgP-graphite composite and copper block were measured by Archimedes' method. The theoretical density was calculated by dividing the bulk density of the sintered composite by the theoretical density calculated from the rule of mixtures using 8.95 g/cm$^3$, and 2.25 g/cm$^3$ as densities for copper and magnesium phosphate, respectively. The hardness was investigated using a Micro Vickers hardness tester (HMV-G, SHIMADZU Corp., Kyoto, Japan) under a load of 0.5 kg with a dwell time of 10 s. Each sample was measured five times, and the data obtained were the average value. The physical properties of the sintered composites are shown in Table 1.

**Table 1.** Physical properties of the copper and the sintered composite blocks.

| **Copper Block** | | **Cu-MgPG Composite Block** | |
|---|---|---|---|
| Bulk density (g/cm$^3$) | 8.89 | Bulk density (g/cm$^3$) | 8.27 |
| Theoretical density (g/cm$^3$) | 8.95 | Theoretical density (g/cm$^3$) | 8.36 |
| Relative density (%) | 99.3 | Relative density (%) | 98.9 |
| Vickers hardness (Hv) | 40.73 | Vickers hardness (Hv) | 54.83 |

The density of sintered samples reached 99% of the theoretical density, which demonstrated the efficiency of the powder metallurgy technology in producing high-density materials. From Table 1, it can also be noted that the addition of graphite increased the hardness of copper materials but decreased the apparent density of the sintered composites.

### 2.3. Friction Coefficient and Wear Test

The friction coefficient and wear sliding tests was carried out in a pin-on-disc tribometer (T-18-0162, NANOVEA Corp., Irvine, CA, USA) in ambient conditions (20 ± 0.5 °C and 45 ± 5% RH). The tribological properties of the prepared composite materials were investigated in a dry sliding test. Counterbodies used in the sliding test are 8 mm diameter polished balls (the average surface roughness is less than 0.01 µm) made from commercially available balls-SiC, $Al_2O_3$, SUJ2 bearing steel (Sato Tekkou Corp., Oita, Japan). The hardness values of SiC, $Al_2O_3$, and SUJ2 balls are 2400 HV, 1600 HV, and 770 HV, respectively, which are obtained from the supplier. Before test, both the composite materials and the counterbody were ultrasonically cleaned in an acetone bath for 10 min. Sliding friction and wear tests were performed with a circular sliding under a load of 10 N and the sliding velocity was 0.1 m/s, the wear track radius was 5 mm, and the total sliding distance was 2000 m. There are no other lubricants added in each sliding test. Figure 2 shows the schematic illustration of the sliding tester. Three tests were performed for each counterbody. The friction coefficients were continuously recorded and the wear volume on each sample disc and counterbody was calculated from the surface profile traces across the wear track using a surface profilometer (Mitutoyo Corp., 178-570-01, Kawasaki, Japan).

The worn volume of the disc ($V_d$, mm$^3$) was calculated according to the following equation [17]:

$$V_d = 2\pi r\left(\frac{S_1 + S_2 + S_3 + S_4}{4}\right)$$

where $S$ (mm$^2$) and $r$ (mm) are the cross-sectional areas of the wear track, each at 90° with respect to the previous one, and sliding radius, respectively.

The worn volume of the ball ($V_b$, mm$^3$) was calculated according to the following equations [17]:

$$V_b = \pi h^2\left(R - \frac{h}{3}\right)$$

$$h = R - \sqrt{R^2 - r_\omega^2}$$

where $h$ (mm) is the height of the removed material, $R$ (mm) is original radius of the ball, and $r_\omega$(mm) is the radius of wear scar on the ball.

The specific wear rate ($WR$, mm$^3$/N·m) was further calculated according to the following equation [17]:

$$WR = \frac{V}{L \cdot S}$$

where $V$ (mm$^3$) is the wear volume of the disc ($V_d$) or ball ($V_b$), $L$ (N) is the normal load, and $S$ (m) is the total sliding distance.

The worn surfaces of sample disc after sliding test were studied by SEM and EDS to identify wear mechanisms.

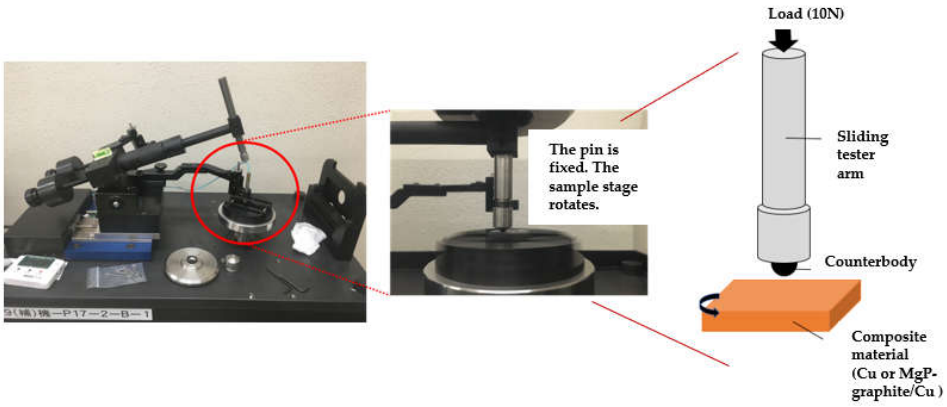


**Figure 2.** Schematic illustration of the pin on disc tester.

### *2.4. Evaluation Method of Worn Surface*

The surface morphology and elemental distribution of the samples were characterized using a scanning electron microscope (SEM, JSM-7500F, JEOL Corp., Tokyo, Japan) equipped with energy dispersive X-ray detector (EDS, JEOL Corp., Tokyo, Japan). Worn surfaces of the samples were also investigated by an X-ray photoelectron spectroscope (XPS) to understand wear-induced surface chemistry modification.

## 3. Results and Discussion

### *3.1. Friction Coefficient and Wear Rate*

Typical evolution of the friction coefficients of copper block sliding against SiC, $Al_2O_3$, and SUJ2 counterbodies at 10 N are shown in Figure 3. All of the friction coefficient diagrams contain two stages such as Figure 3, named the (1) run-in and (2) steady state stage. In the run-in stage, the friction coefficient shows a large and irregular increase and decrease for a period of time; in the steady-state stage, the friction coefficient oscillates continuously within a certain range. The formation of the run-in state stage may be related to the increase of the contact area, the work hardening effect of wear and the accumulation of debris at the pin-disk interface, and the change of the wear mechanism from two-body wear to three-body wear [18]. The reported friction coefficient in this study is the average of these data in the steady stage.

An initial run-in period followed by a steady-state period was observed in all of the tribopairs, while in the run-in stage, the friction coefficient of copper block fluctuates within certain range in a fluctuating manner against SiC, SuJ2, and $Al_2O_3$. The friction coefficient of copper block changed in the range of 0.65–0.85 against SiC, $Al_2O_3$, and SUJ2 counterbodies. When sliding against different counterbodies, the Cu/$Al_2O_3$ tribopair has the lowest coefficient of friction. Cu/SiC tribopair showed the highest friction coefficient in the steady-state period.

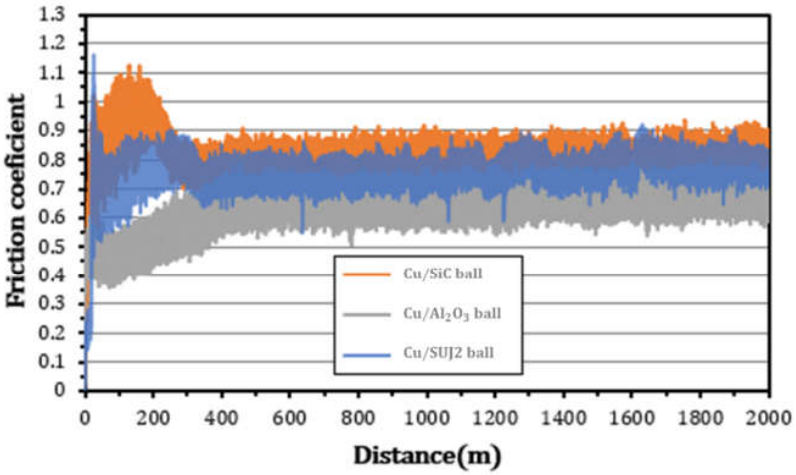


**Figure 3.** Evolution of friction coefficients of copper block sliding against SiC, $Al_2O_3$, and SUJ2 counterbodies at 10 N.

Typical evolution of the friction coefficients of Cu-MgPG composites sliding against SiC, $Al_2O_3$, and SUJ2 counterbodies at 10 N are shown in Figure 4. The average friction coefficients of all of the tribopairs in steady-state period are summarized in Figure 5.

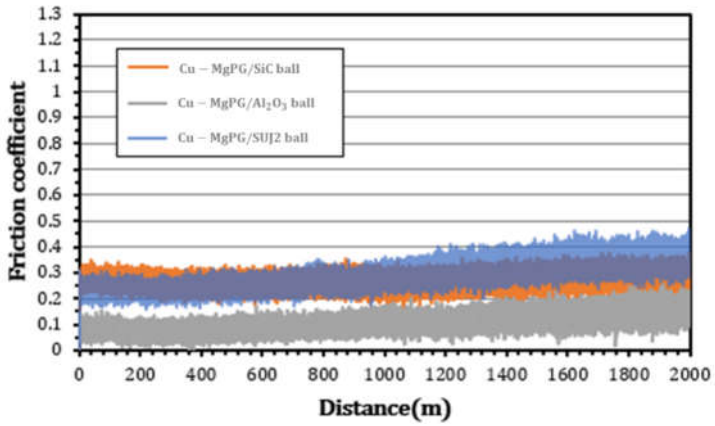


**Figure 4.** Evolution of friction coefficients of copper/MgP-graphite composites sliding against SiC, $Al_2O_3$, and SUJ2 counterbodies at 10 N.

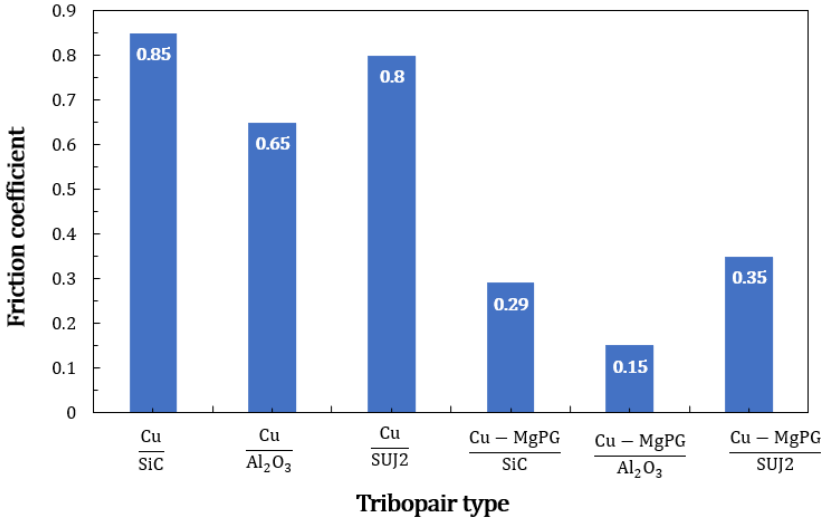


**Figure 5.** The average friction coefficients of tribopairs.

The friction coefficient detected with the tribopairs of Cu-MgPG composite material is significantly lower than that of the pure copper material. The friction coefficient of Cu-MgPG composites changed in the range of 0.15–0.35 against SiC, $Al_2O_3$, and SUJ2 counterbodies. Similar to the results of copper tribopair, Cu-MgPG/$Al_2O_3$ tribopair has the lowest coefficient of friction. However, the Cu-MgPG/SUJ2 tribopair showed the highest friction coefficient in the steady-state period.

From Figure 5, it can be noted that the addition of magnesium phosphate treated graphite decreased the friction coefficient of the sintered composites against each counterbody.

The specific wear rate (*WR*) of the sintered disc is displayed in Figure 6, and the results showed WR of sintered copper discs changed in the range of $3.13 \times 10^{-6}$–$6.27 \times 10^{-6}$ $mm^3/N{\cdot}m$ against $Al_2O_3$, SiC, and SUJ2 counterbodies at a load of 10 N.

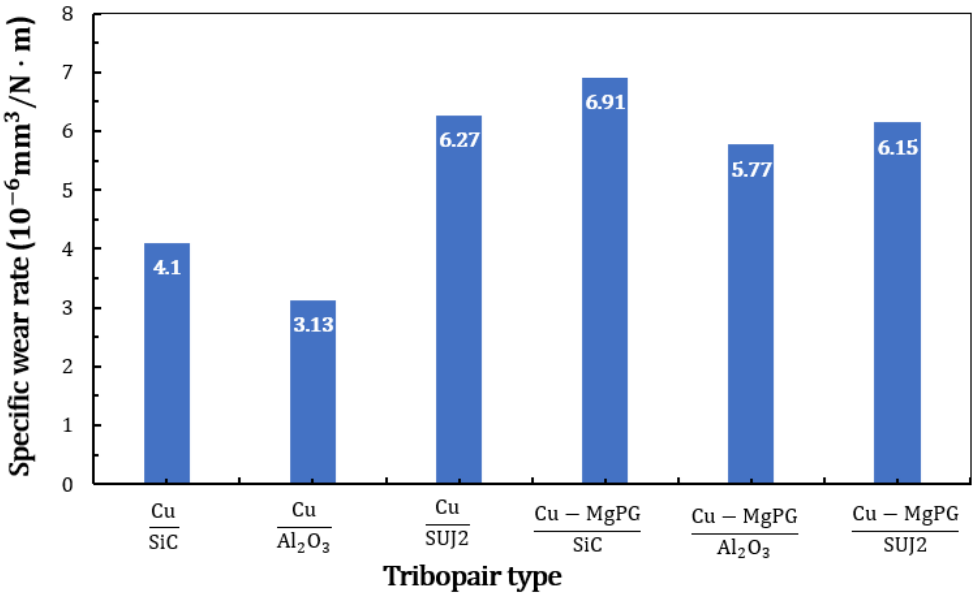


**Figure 6.** Average specific wear rate of the sintered disc against SiC, $Al_2O_3$, SUJ2 counterbodies.

For the sintered copper disc, the lowest wear rate disappeared when sliding against $Al_2O_3$ counterbody, which is similar to the relationship of the friction coefficient. However, the highest WR disappeared when sliding against SUJ2 counterbody that is different with the result of the friction coefficient. In addition, the WR results with sintered Cu-MgPG disc also shows that the lowest wear rate and highest wear rate disappeared when sliding against $Al_2O_3$ and SUJ2 counterbody, respectively. Considering the data in Figures 5 and 6, the specific wear rate of the sintered disc against SiC, $Al_2O_3$, SUJ2 counterbodies didn't show obvious dependence on their friction coefficients. At the same time, even though the average friction coefficient of the sintered Cu-MgPG composite materials decreased significantly with sintered copper materials, the specific wear rate increased instead when sliding against SiC and $Al_2O_3$ ball.

The average specific wear rates of SiC, $Al_2O_3$, SUJ2 counterbodies with two sintered discs are summarized in Figure 7.

It can be found from Figure 7 that $Al_2O_3$ ball exhibited lower specific wear rate when sliding against two kinds of sintered disc compared with other counterbodies. The specific wear rate of SiC ball was the highest when sliding against sintered Cu-MgPG composite materials which is corresponding to the result shown in Figure 6. From the comparison between Figures 6 and 7, it is clear that the specific wear rates between the sintered disc and counterbodies were consistent.

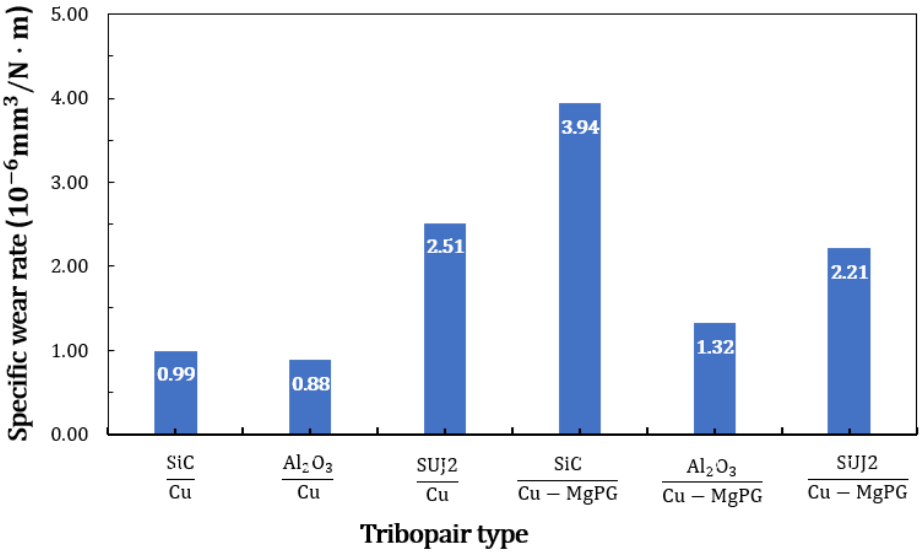


**Figure 7.** Average specific wear rates of SiC, $Al_2O_3$ and SUJ2 counterbodies with different sintered disc.

### *3.2. The Morphology Analysis of Worn Surface*

Figure 8 shows the morphologies of worn surfaces of the sintered discs after sliding tests with different counterbody. The corresponding elemental analysis results (EDS) are shown in Figure 9.

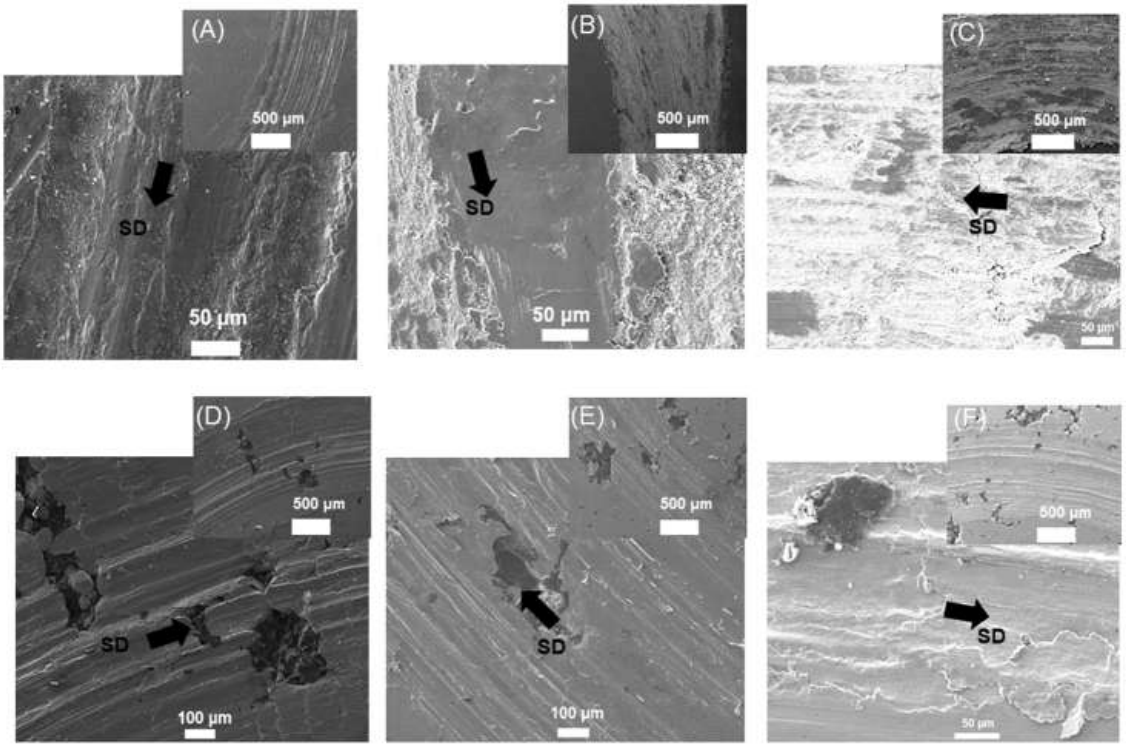


**Figure 8.** SEM morphology of the worn surface of the sintered discs that sliding against different counterbodies (**A**) Cu/$Al_2O_3$; (**B**) Cu/SiC; (**C**) Cu/SuJ2; (**D**) Cu-MgPG/$Al_2O_3$; (**E**) Cu-MgPG/SiC; (**F**) Cu-MgPG/SuJ2.

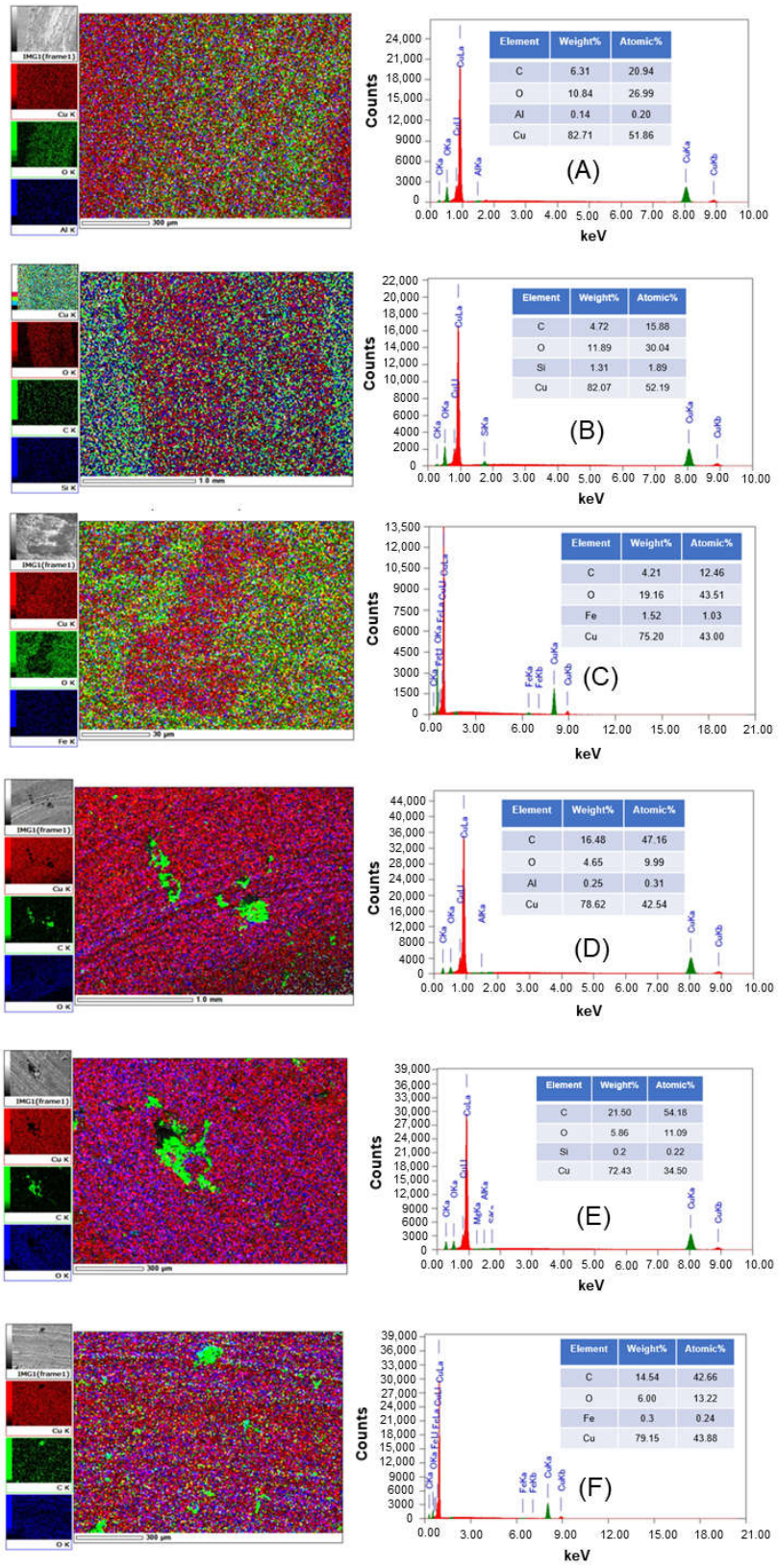


**Figure 9.** EDS analysis of the worn surface of the sintered discs that sliding against different counterbodies (**A**) Cu/$Al_2O_3$; (**B**) Cu/SiC; (**C**) Cu/SuJ2; (**D**) Cu-MgPG/$Al_2O_3$; (**E**) Cu-MgPG/SiC; (**F**) Cu-MgPG/SuJ2.

Figure 8A–C displayed the worn surface of the sintered copper sample. While Figure 8D–F displayed the worn surface of the sintered Cu-MgPG sample. It can be seen that after the sliding experiment, the worn surface left on the sintered Cu-MgPG sample is different from sintered copper sample. Clear grooves appear on the wear surface of the graphite-added sintered samples. From the analysis of the results of EDS (Figure 9), it can be inferred that the formation of these grooves is related to the oxides formed on the surface.

In addition, SEM images of Figure 8 D, E showed that there was a partial detachment of graphite form the inner region of the pockets. For the samples with graphite addition, graphite particles agglomerate in regions between Cu matrix grains, stored in pockets with internal voids [19]. At the same time, it indicates that the reduced density and low theoretical density (as shown in Table 1) of the graphite-containing samples is associated with the internal voids in pockets of graphite present in the composites. Meanwhile, in Figure 8F, graphite particles staying on the worn surface are observed, which are presumably exposed from the graphite-storing voids during the friction process.

Elemental analysis of all samples after sliding experiments showed the presence of a large amount of oxygen on the wear track. However, material shedding, plastic deformation and numerous grooves can be clearly seen on the wear track of the graphite added sintered samples. There are only a few grooves on the wear track surface of the sintered copper sample. This proves that different oxides are formed on the surface of the two samples. No obvious graphite film formation was observed in the EDS mapping in Figure 9D,E, but observed on the wear track formed by the Cu-MgPG/SuJ2 tribopair shown in Figure 9F, there are some linear tracks formed by the graphite element.

According to the results in Figure 5, it can be known that the lowest friction coefficient of sintered disc appeared when sliding against $Al_2O_3$ counterbody, while the hardness of the $Al_2O_3$ ball is in the middle of the other two counterbodies. It was proved that the hardness of the counterbody is not the key to determining the friction coefficient. Combined with the EDS results, it is assumed that the reduction in the average friction coefficient of $Cu/Al_2O_3$ and $Cu\text{-}MgPG/Al_2O_3$ tribopairs should be related to the oxides produced on the worn surface during the friction process.

XPS results in Figures 10 and 11 were also conducted on the sintered copper sample and sintered Cu-MgPG sample surfaces after sliding against different counterbodies to confirm the oxidation in sliding. Results from XPS analysis for $Al_{2p}$, $O_{1s}$, $C_{1s}$ core levels obtained on the worn surface of sintered samples sliding against $Al_2O_3$ counterbody are provided in Figure 10.

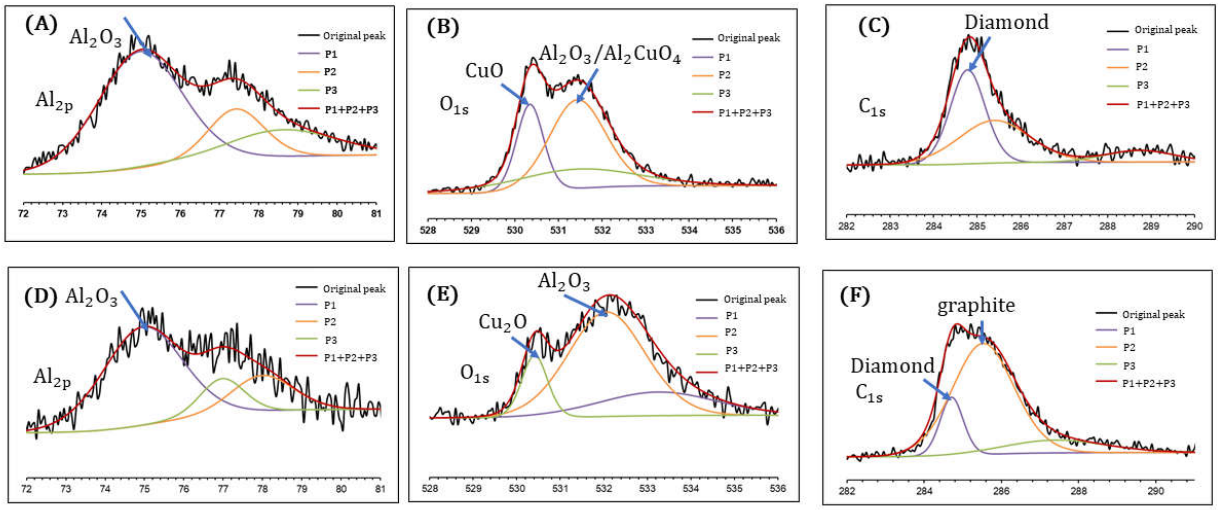


**Figure 10.** XPS analysis of worn surfaces of sintered copper samples (**A**–**C**) and sintered Cu-MgPG samples (**D**–**F**) against $Al_2O_3$ counterbody.

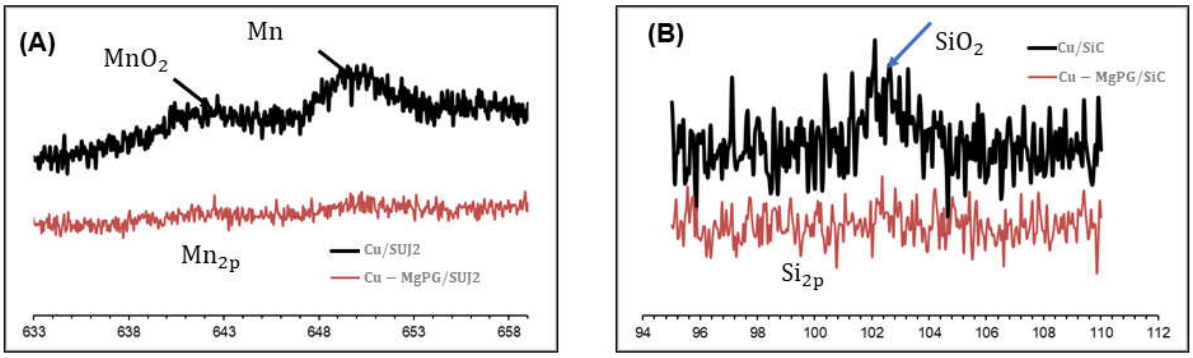


**Figure 11.** XPS analysis of worn surfaces of sintered copper and Cu-MgPG samples against (**A**) SUJ2 counterbody; (**B**) SiC counterbody.

As shown in Figure 10A,D, the $Al_{2p}$ peak($P_1$ + $P_2$ + $P_3$) fitted to the original peak is composed of three peaks P1, P2, P3 (as revealed by Gaussian curve fitting), each of which are assigned to different bonds containing Al. The $Al_{2p}$ peak at 75 eV corresponds to the presence of $Al_2O_3$ [20]. Meanwhile, there are also two unknown peaks appeared in copper sample and Cu-MgPG sample. The fitted $O_{1s}$ peak was deconvoluted into three parts using Gaussian curve fitting. The two main $O_{1s}$ peak at 530.35 eV and 531.4 eV appeared in Figure 10B correspond to the presence of CuO [21] and $Al_2O_3$ [22] or $Al_2CuO_4$ [23] respectively. While as shown in Figure 10E, the $O_{1s}$ peak at 530.2 eV corresponds to the presence of $CuO_2$ [24], $O_{1s}$ peak at 532.0 eV belongs to $Al_2O_3$ [25]. The C element in the EDS results (Figure 9A) indicates that there is also carbon in the wear surface of the pure copper sample. After the analysis of $C_{1s}$ by XPS, the fitted $C_{1s}$ peak was deconvoluted into three separate peaks using Gaussian curve fitting. $C_{1s}$ peak at 284.8 eV as shown in Figure 10C, and 284.9 eV as shown in Figure 10F corresponds to the presence of diamond structure [26,27]. It can be speculated that there are some abrasive particles (diamond) remaining after the copper sample is polished. In addition, the $C_{1s}$ peak at 285.7 eV in Figure 10F corresponds to the presence of graphite [28]. This proves that during the friction process, there are graphite particles exposed from the graphite-storing voids and stay on the friction contact surface.

XPS analysis of worn surfaces of copper and Cu-MgPG composite materials against SuJ2 counterbody and SiC counterbody is shown in Figure 11. Compared with the analysis results of EDS (as shown in Figure 9C), the presence of Mn element was detected on the wear surface with XPS analysis (Figure 11A) after the copper sample sliding against SUJ2 counterbody. It can be speculated that the Mn element comes from the debris of the SUJ2 counterbody remaining on the disc surface. The $Mn_{2p}$ peak at 642.2 eV corresponds to the presence of $MnO_2$ [29] and the peak at 650.0 eV corresponds to the presence of Mn [30]. However, the peak representing the Mn element is not significant on the Cu-MgPG sample. The $Si_{2p}$ peak at 103.1 eV corresponds to the presence of $SiO_2$ [31]. The peak representing the Si element is not significant on the Cu/MgPG sample.

Combined with the results of the Specific wear rate shown in Figures 6 and 7, it can be speculated that the sliding test with Cu-MgPG sample against SUJ2 counterbody can reduce the average friction coefficient while reducing wear.

## 4. Conclusions

In this study, a Cu-MgPG material was prepared, and the experimental results proved that the Cu-MgPG material in this study has self-lubricating properties. In addition, under fixed experimental conditions (fixed load 10 N and sliding speed 0.1 m/s), the optimum tribopair combination of Cu and Cu-MgPG with the counterbody material, the influence of the counterbody materials in terms of coefficient of friction and wear was examined, and the following findings were obtained.

(1) The friction coefficient detected with the tribopairs of Cu-MgPG composite material is significantly lower than that of the pure copper material since the added graphite acts as a solid lubricant.

(2) The Cu-MgPG/SUJ2 pair was found to decrease both the friction coefficient and specific wear amount compared to the Cu/SUJ2 pair. From the results of XPS and EDS analysis of the sliding surfaces, it is considered that the added MgPG acted as a solid lubricant and suppressed the oxidation behavior of the material. On the other hand, the Cu-MgPG/$Al_2O_3$ pair was found to have the lowest coefficient of friction and specific wear of all of the pairs.

In general, the results of this study have demonstrated the application potential of Cu/MgPG materials under specific circumstances. However, in the case of practical application, there are changes in loads and sliding speeds, so the materials prepared in this study cannot be immediately put into the application of brush or bearing materials. In future research, it is necessary to continue studying the effects of sliding loads and sliding speeds on the coefficient of friction and wear with different tribopairs.

**Author Contributions:** Data curation, R.L.; investigation, R.L.; writing-original draft, R.L.; methodology, S.Y.; resources, H.K. and K.Y.; writing—review and editing, S.Y. and K.Y.; supervision, S.Y. and H.K.; project administration, H.K.; funding acquisition, H.K. All authors have read and agreed to the published version of the manuscript.

**Funding:** This research received no external funding.

**Institutional Review Board Statement:** Not applicable.

**Informed Consent Statement:** Not applicable.

**Data Availability Statement:** The data presented in this study are available in this article.

**Acknowledgments:** This work was financially supported by JST SPRING, Grant Number JPMJSP2125. The author (Initial) would like to take this opportunity to thank the "Interdisciplinary Frontier Next-Generation Researcher Program of the Tokai Higher Education and Research System." This work was partly supported by the DII Collaborative Graduate Program for Accelerating Innovation in Future Electronics, Nagoya University.

**Conflicts of Interest:** The authors declare no conflict of interest.

## References

1. Kestursatya, M.; Kim, J.; Rohatgi, P. Wear performance of copper–graphite composite and a leaded copper alloy. *Mater. Sci. Eng. A* **2003**, *339*, 150–158. [CrossRef]
2. Kato, H.; Takama, M.; Iwai, Y.; Washida, K.; Sasaki, Y. Wear and mechanical properties of sintered copper–tin composites containing graphite or molybdenum disulfide. *Wear* **2003**, *255*, 573–578. [CrossRef]
3. Rohatgi, P.K.; Ray, S.; Liu, Y. Tribological properties of metal matrix-graphite particle composites. *Int. Mater. Rev.* **1992**, *37*, 129–152. [CrossRef]
4. Kováčik, J.; Emmer, Š.; Bielek, J.; Keleši, L. Effect of composition on friction coefficient of Cu–graphite composites. *Wear* **2008**, *265*, 417–421. [CrossRef]
5. Kumar, R.; Antonov, M. Self-lubricating materials for extreme temperature tribo-applications. *Mater. Today Proc.* **2021**, *44*, 4583–4589. [CrossRef]
6. Zhao, J.; Liu, Y.; Liu, D.; Gu, Y.; Zhang, R.; Ma, R.; Li, S.; Wang, Y.; Shi, Y. The Tribological Performance of Metal-/Resin-Impregnated Graphite under Harsh Condition. *Lubricants* **2022**, *10*, 2. [CrossRef]
7. Yasar, I.; Canakci, A.; Arslan, F. The effect of brush spring pressure on the wear behaviour of copper–graphite brushes with electrical current. *Tribol. Int.* **2007**, *40*, 1381–1386. [CrossRef]
8. Mazloum, A.; Kováčik, J.; Zagrai, A.; Sevostianov, I. Copper-graphite composite: Shear modulus, electrical resistivity, and cross-property connections. *Int. J. Eng. Sci.* **2020**, *149*, 103232. [CrossRef]
9. Sarmadi, H.; Kokabi, A.; Reihani, S.S. Friction and wear performance of copper–graphite surface composites fabricated by friction stir processing (FSP). *Wear* **2013**, *304*, 1–12. [CrossRef]
10. Xiao, Y.; Zhang, Z.; Yao, P.; Fan, K.; Zhou, H.; Gong, T.; Zhao, L.; Deng, M. Mechanical and tribological behaviors of copper metal matrix composites for brake pads used in high-speed trains. *Tribol. Int.* **2018**, *119*, 585–592. [CrossRef]
11. Zhan, Y.; Zhang, G. The role of graphite particles in the high-temperature wear of copper hybrid composites against steel. *Mater. Des.* **2006**, *27*, 79–84. [CrossRef]

12. Li, R.; Yamashita, S.; Kita, H. Investigating the chemical bonding state of graphite powder treated with magnesium(II) phosphate through EELS, TEM, and XPS analysis. *Diam. Relat. Mater.* **2021**, *116*, 108423. [CrossRef]
13. Moustafa, S.; El-Badry, S.; Sanad, A.; Kieback, B. Friction and wear of copper–graphite composites made with Cu-coated and uncoated graphite powders. *Wear* **2002**, *253*, 699–710. [CrossRef]
14. Xia, J.-T.; Hu, Z.-L.; Chen, Z.-H.; Ding, G.-Y. Preparation of carbon brushes with thermosetting resin binder. *Trans. Nonferrous Met. Soc. China* **2007**, *17*, 1379–1384. [CrossRef]
15. Liu, J.; Sun, K.; Zeng, L.; Wang, J.; Xiao, X.; Liu, J.; Guo, C.; Ding, Y. Microstructure and Properties of Copper–Graphite Composites Fabricated by Spark Plasma Sintering Based on Two-Step Mixing. *Metals* **2020**, *10*, 1506. [CrossRef]
16. Opálek, A.; Emmer, Š.; Čička, R.; Beronská, N.; Oslanec, P.; Kováčik, J. Structure and Thermal Expansion of Cu−90 vol. % Graphite Composites. *Materials* **2021**, *14*, 7089. [CrossRef]
17. Zhang, W.; Yamashita, S.; Kita, H. Effect of counterbody on tribological properties of B4C–SiC composite ceramics. *Wear* **2020**, *458–459*, 203418. [CrossRef]
18. Zhang, Y.; Han, Z.; Wang, K.; Lu, K. Friction and wear behaviors of nanocrystalline surface layer of pure copper. *Wear* **2006**, *260*, 942–948. [CrossRef]
19. Su, Y.; Zhang, Y.; Song, J.; Hu, L. Tribological behavior and lubrication mechanism of self-lubricating ceramic/metal composites: The effect of matrix type on the friction and wear properties. *Wear* **2017**, *372–373*, 130–138. [CrossRef]
20. Kim, Y.-C.; Park, H.-H.; Chun, J.S.; Lee, W.-J. Compositional and structural analysis of aluminum oxide films prepared by plasma-enhanced chemical vapor deposition. *Thin Solid Film.* **1994**, *237*, 57–65. [CrossRef]
21. Rueda, F.; Mendialdua, J.; Rodriguez, A.; Casanova, R.; Barbaux, Y.; Gengembre, L.; Jalowiecki, L. Characterization of Venezuelan laterites by X-ray photoelectron spectroscopy. *J. Electron Spectrosc. Relat. Phenom.* **1996**, *82*, 135–143. [CrossRef]
22. Zhdan, P.; Shepelin, A.; Osipova, Z.; Sokolovskii, V. The extent of charge localization on oxygen ions and catalytic activity on solid state oxides in allylic oxidation of propylene. *J. Catal.* **1979**, *58*, 8–14. [CrossRef]
23. Klein, J.C.; Li, C.P.; Hercules, D.M.; Black, J.F. Decomposition of Copper Compounds in X-ray Photoelectron Spectrometers. *Appl. Spectrosc.* **1984**, *38*, 729–734. [CrossRef]
24. Dubé, C.E.; Workie, B.; Kounaves, S.P.; Robbat, A., Jr.; Aksub, M.L.; Davies, G. Electrodeposition of Metal Alloy and Mixed Oxide Films Using a Single-Precursor Tetranuclear Copper-Nickel Complex. *J. Electrochem. Soc.* **1995**, *142*, 3375. [CrossRef]
25. Dua, A.; George, V.; Agarwala, R. Characterization and microhardness measurement of electron-beam-evaporated alumina coatings. *Thin Solid Film.* **1988**, *165*, 163–172. [CrossRef]
26. Lau, W.M.; Huang, L.J.; Bello, I.; Yiu, Y.M.; Lee, S. Modification of surface band bending of diamond by low energy argon and carbon ion bombardment. *J. Appl. Phys.* **1994**, *75*, 3385. [CrossRef]
27. Schmieg, S.J.; Belton, D.N. Polycrystalline Diamond Film on Si(100) by XPS. *Surf. Sci. Spectra* **1992**, *1*, 329. [CrossRef]
28. Hrbek, J. Carbonaceous overlayers on Ru(001). *J. Vac. Sci. Technol. A* **1986**, *4*, 86. [CrossRef]
29. Tan, B.J.; Klabunde, K.J.; Sherwood, P.M.A. XPS studies of solvated metal atom dispersed (SMAD) catalysts. Evidence for layered cobalt-manganese particles on alumina and silica. *J. Am. Chem. Soc.* **1991**, *113*, 855–861. [CrossRef]
30. Jenks, C.J.; Chang, S.-L.; Anderegg, J.W.; Thiel, P.A.; Lynch, D.W. Photoelectron spectra of anAl70Pd21Mn9quasicrystal and the cubic alloyAl60Pd25Mn15. *Phys. Rev. B* **1996**, *54*, 6301–6306. [CrossRef]
31. Yan, Y.; Helfand, M.; Clayton, C. Evaluation of the effect of surface roughness on thin film thickness measurements using variable angle XPS. *Appl. Surf. Sci.* **1989**, *37*, 395–405. [CrossRef]